Research Article Vol. 59, No. 10 / 1 April 2020 / Applied Optics 3049

applied optics

Optical design of the visible telescope for the SVOM mission

Xuewu Fan,[1] Gangyi Zou,[1,2,*] Yulei Qiu,[3] Zhihai Pang,[1] Hui Zhao,[1] Qinfang Chen,[1] Yue Pan,[1,2] and Hao Yuan[1]

[1]Space Optics Laboratory, Xi'an Institute of Optics and Precision Mechanics, Chinese Academy of Sciences, Xi'an 710119, China
[2]University of Chinese Academy of Sciences, Beijing 100049, China
[3]National Astronomical Observatories, Chinese Academy of Sciences, Beijing 100012, China
*Corresponding author: zougangyi@opt.ac.cn

Received 18 December 2019; revised 24 February 2020; accepted 29 February 2020; posted 2 March 2020 (Doc. ID 386177); published 25 March 2020

This paper describes the optical design of the visible telescope (VT), which is the primary payload for the Chinese-French Space-based multi-band astronomical Variable Objects Monitor (SVOM) mission, for the detection and observation of high-redshift gamma-ray bursts. The VT aims at reaching a limiting magnitude of +22.5 Mv with the exposure time of 300 s in the 630 km Sun-synchronous orbit with an inclination of 30°. The VT, also known as the fine guidance sensor for the SVOM, aims to measure the relative performance error (RPE) of the platform during the tracking and provide the RPE to the platform to correct its stability. The optical design is presented in this paper. The mirror manufacture and test results are presented. The optical system performance, tolerance budget, thermal analysis, and stray light design of VT are fully analyzed. Finally, the diffraction encircled energy and point source transmittance are tested in the lab for the finished telescope.

https://doi.org/10.1364/AO.386177

1. INTRODUCTION

The Space-based multi-band astronomical Variable Objects Monitor (SVOM) is a dedicated satellite developed within the framework of a collaboration between China and France for detection, localization, and observation of gamma-ray bursts (GRBs) and other high-energy transient astronomical events [1,2]. The visible telescope (VT), together with a wide field-of-view camera (ECLAIRs) [3], a soft x-ray telescope (MXT) [4], and a gamma-ray burst monitor [1,2], will detect the GRBs and prompt emission, rapidly localizing their position with the accuracy from arcminutes to arcseconds.

The main task of the VT is to observe the afterglows of GRBs both in the visible and near-infrared and provide redshift estimation and some promising candidates at the early time for the ground-based large telescopes. Another task of the VT is to measure the relative performance error (RPE) of the satellite, aiming to improve the pointing stability of the platform during observation. Two additional fine guidance sensors (FGSs) are mounted on the visible focal plane of the VT besides the main CCD to measure the image shifts and rotations. The VT has been designed, manufactured, and tested by a team involving the Xi'an Institute of Optics and Precision Mechanics and the National Astronomical Observatories of China.

In this paper optical design of the VT telescope and its performance are presented. In particular, the optical system design strategy and its main characters are presented in Section 2. Section 3 describes the optical performance of the optical system. A detailed tolerance error budget is presented in Section 4. Section 5 describes the optimal working temperature range to provide the prime requirement for thermal control of the VT. The stray light design, analysis, and simulation are presented in Section 6. Section 7 shows the optical performance validation in the lab. In Section 8, conclusions on the VT optical design are presented.

2. OPTICAL DESIGN AND MANUFACTURING

The scientific observation requires the VT to reach a limiting magnitude of +22.5 Mv with the exposure time of 300 s and provide the redshift indicators for high-Z ($z > 6$) GRBs. The satellite engineering needs the VT to provide the RPE measurement of the satellite with a precision of 0.2 arc sec. These requirements derive a list of stringent optical specifications for the VT, which is summarized in Table 1.

A. Optical Design

The pupil diameter of the VT is 440 mm, which is too large for a dioptric system due to the limitation of optical materials. Only catadioptric or all-reflective optical system configurations were considered. As two FGSs are mounted on the blue band

Table 1. Optical Specifications for VT

Parameters	Description
Optical configuration	Catadioptric Ritchey–Chrétien
Pixel resolution	0.77 arc sec/pixel
Pupil diameter	440 mm
Focal length	3600 mm
Field of view	≥ 26 arcmin × 26 arcmin ≥ 12.7 arcmin × 12.7 arcmin (FGS)
Spectral range	400 nm–650 nm (blue band) 650 nm–1000 nm (red band) 400 nm–650 nm (FGS)
Surface obscuration	0.18
Optical transmission	0.6 (average)
Detector	2048 × 2048 pixels, 13.5 μm × 13.5 μm 1024 × 1024 pixels, 13 μm × 13 μm (FGS)
Diameter of 80% EE (blue band)	≤ 2 pixels
Diameter of 70% EE (red band)	≤ 2 pixels
Diameter of 80% EE (FGS)	≤ 3 pixels
Stray light	< 1/3 sky background when the Moon is > 30 deg off axis

focal plane of the VT, the circular field of view (FOV) should be no less than 1.39°, which is too large for an on-axis two-mirror optical system to correct all the aberrations. An on-axis or off-axis three mirror anastigmatic (TMA) optical system can be adopted but will make the optical system complicated. Consequently, the optical configuration of the VT (Fig. 1) is based on a catadioptric optical design and adopts a Ritchey–Chrétien (RC) configuration with dedicated correctors and an ingenious dichromatic ray-splitting prism [5,6].

The primary mirror (PM) is a conic surface not far from a parabola and the secondary mirror (SM) is a hyperboloid. In order to correct the residual aberration of the RC configuration, the VT adopts three lenses near the back of the PM and the first two lenses are servo-controlled along the optical axis to adjust focus, which is necessary for the VT to keep the optical performance in orbit. Then an ingenious dichroic prism ray-splitter is inserted before the focal plane to ensure the VT can take observations in the blue band and red band simultaneously. The vacuum windows for ground performance tests are also taken into consideration. Fused silica is used for the first lens and vacuum windows, while HLAK3 is used for the other two lenses and HZK3 is used for the prism. All the glass materials are radiation proof for space application.

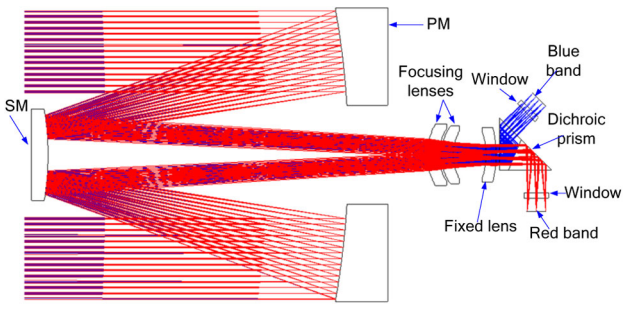

Fig. 1. Schematic optics layout of the VT.

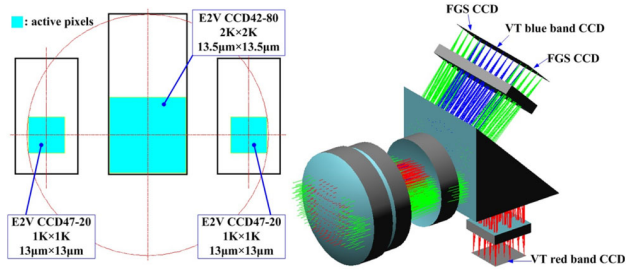

Fig. 2. CCDs arrangement (left) and positions (right) on the blue band focal plane.

In order to improve the pointing precision of the satellite attitude control system, two FGSs are mounted on the blue band focal plane of the VT. The preferred CCD for the VT is the back-illuminated high-performance E2V CCD42-80 full frame CCD without a window, which operates in the frame transfer mode. The pixel size is 13.5 μm × 13.5 μm and the array size is 2 K × 2 K. The E2V CCD47-20 has been chosen to be the FGS sensor, whose pixel size is 13 μm × 13 μm and the array size is 1 K × 1 K. The CCD47-20 has a 1.5 mm thick NBK7 window. The CCDs arrangement on the focal plane is shown in Fig. 2. The minimum diameter of the circle that enclosed the CCDs is 87.69 mm, so the design circular FOV of the VT should be no less than 1.39°. Finally, the design circular FOV of the VT is 1.4° for the blue band, while the design circular FOV for the red band is 0.63°.

Figure 3 shows the dichroic ray-splitting method. It is just like a 45° right angle prism, divided into a half-penta prism and the remain part. The rays of the blue band are reflected, while the rays of the red band are refracted at the dichroic splitting surface. The glass type of the prism has been selected carefully to make sure the beam can be totally internal reflected (TIR) at the TIR surface.

Distances between optical elements have been managed to achieve a satisfactory package. The final design envelope is Φ450 mm × 760 mm, excluding the external baffle. To reduce the light loss due to the central obscuration, the diameter of SM

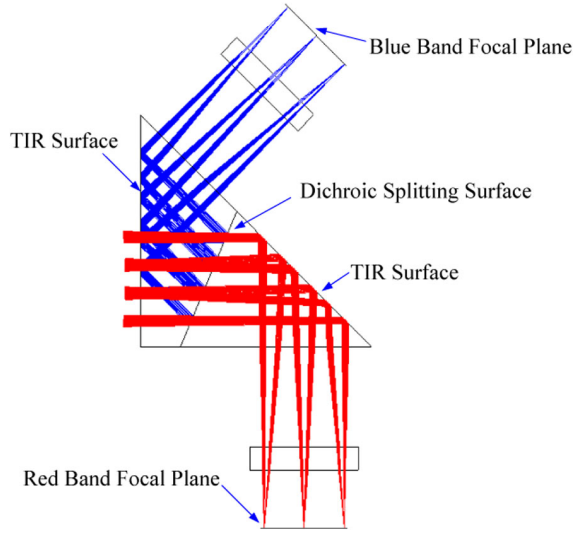

Fig. 3. Prism design and ray splitting concept.

has been minimized to about 30% (in diameter), with respect to the PM.

B. Mirrors

The material of the PM and SM both adopt SiC. Figure 4 shows the lightweight design method of the Φ440 mm primary mirror, which adopts single arch, open-back, and triangle holes to reduce its weight. The Φ135 mm secondary mirror also adopts open-back and triangle holes to reduce its weight. The mirrors have been coated with a thin layer of silicon before the fine polishing stage in order to improve the surface roughness and reflectance.

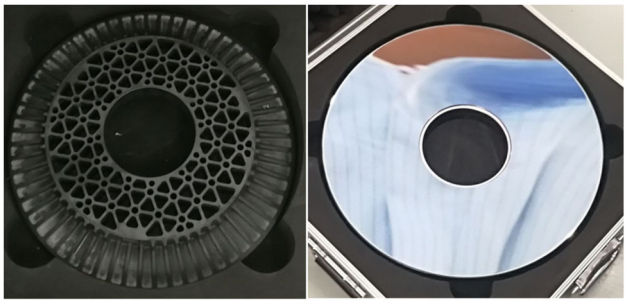

Fig. 4. Bottom view (left) and top view (right) of the finished PM.

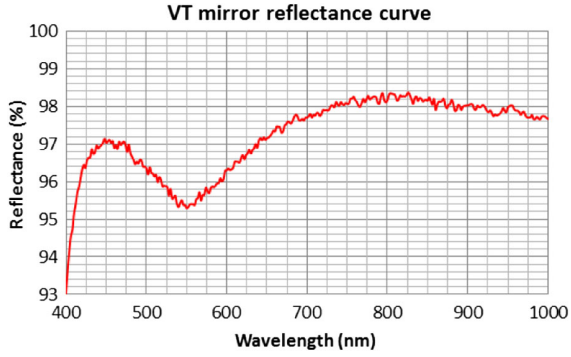

Fig. 5. VT mirror reflectance curve.

Fig. 6. RMS figure error of the PM with coating.

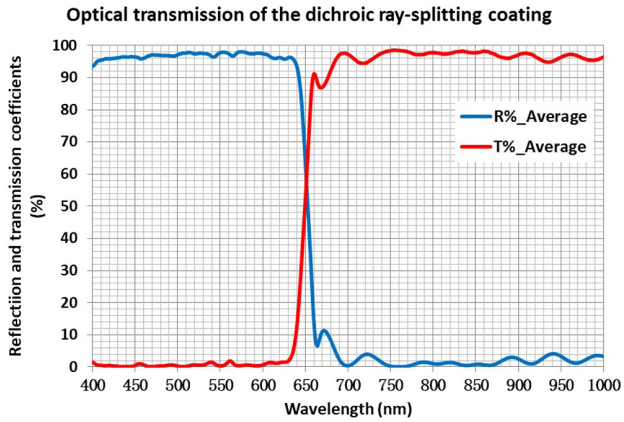

Fig. 7. Optical transmission curve of the dichroic ray-splitting coating.

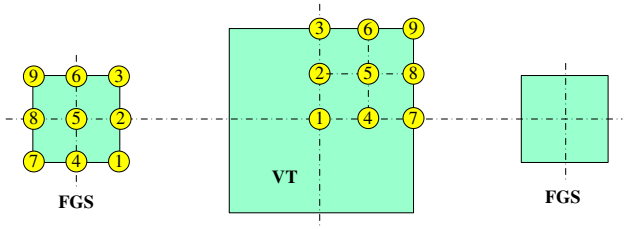

Fig. 8. FOV points of the VT and FGS for optical performance analysis.

An enhanced high-reflectivity Ag-protected coating is adopted and the reflectance curve is shown in Fig. 5.

Figure 6 shows the RMS figure error of the PM tested by the ZYGO interferometer, which is less than $\lambda/50$ ($\lambda = 632.8$ nm). The RMS figure error of the SM has also been tested, which is less than $\lambda/80$ ($\lambda = 632.8$ nm).

C. Dichroic Coating

The optical transmission of the dichroic coating is shown in Fig. 7. The average values of reflection and transmission coefficients are both larger than 95% and meet the scientific requirement.

Considering the obstruction loss caused by the SM assembly, the final optical transmissions of the VT are no less than 60% (average) both for the blue and red bands.

3. OPTICAL PERFORMANCE

Code V has been used for the optical design and analysis. For optical performance analysis, nine FOV points are chosen both

Table 2. VT Main Optical Performance

FOV	Diameter of 80% or 70% EE (Pixel)	Maximum Distortion
Blue band of VT	1.29–1.43 (80%)	0.11%
Red band of VT	1.56–1.60 (70%)	0.11%
FGS	1.68–2.21 (80%)	0.98%

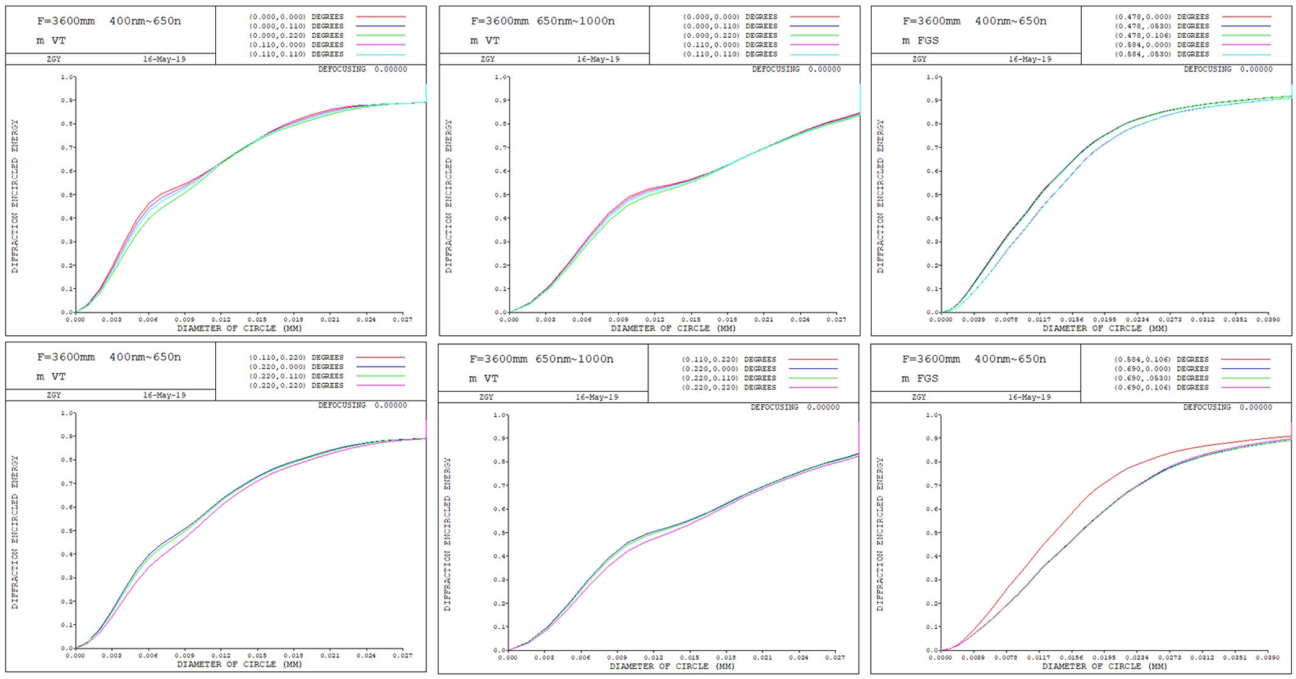

Fig. 9. Curves of diffraction EE of the nominal design: blue band of the VT (left), red band of the VT (middle), and the FGS (right).

for the VT and FGS considering the symmetry of optics and are shown in Fig. 8. Those FOV points can fully descript the optical performance of the VT.

The fraction of diffraction encircled energy (EE) has been considered to evaluate the image quality. In addition, the distortion and RMS spot diameter have been evaluated. The performance loss caused by the central obscuration has been included in the analyses. Table 2 shows the main optical performance of the VT.

Figure 9 shows the curves of diffraction EE for the VT and FGS. The optical system has achieved diffraction-limited performance in the FOV for the VT. The diameters of 80% EE for the blue band of the VT are smaller than 1.43 pixels and the diameters of 70% EE for the red band of the VT are smaller than 1.6 pixels. The diameters of 80% EE for the FGS are all smaller than 2.21 pixels.

The relative distortion grid for the whole FOV of the telescope is shown in Fig. 10. The maximum relative distortion is 0.98% at the edge of the FOV for the FGS, and for the VT the maximum distortion is no more than 0.11%.

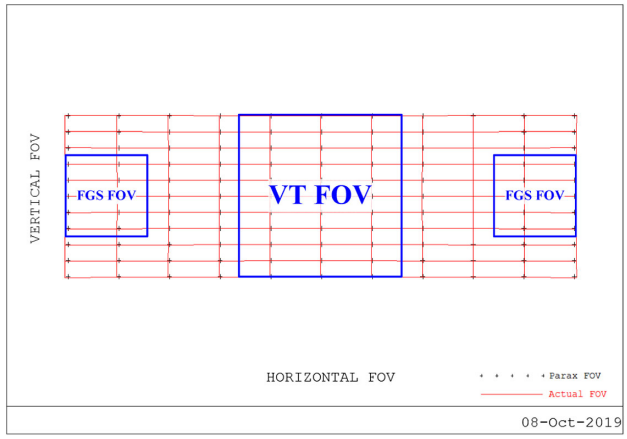

Fig. 10. Distortion grid for the whole FOV.

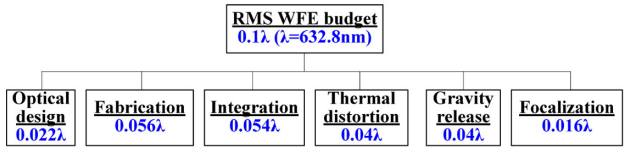

Fig. 11. RMS WFE budget.

4. TOLERANCE ANALYSIS

A detailed error budget is needed to keep track of all factors that affect the optical performance and attain a balance among tolerances so that each of them can be achieved. Figure 11 shows the breakdown of the RMS wavefront error (WFE) budget at various phases of the fabrication, integration, test, launch, and on-orbit operations. In order to meet the required performance of EE, the RMS WFE must be no more than 0.1λ [7].

A tolerance budget is given after studying the sensitivity of the diffraction EE to variations of optical element parameters, such as curvatures, shapes, locations, and orientations. The most sensitive tolerance is the distance between the PM and the SM, due to the 5.8× magnification between the telescope and the PM focal length and the defocus of 36×, which means a displacement of 1 μm between the PM and the SM produces a defocus of 36 μm [8].

The ranges for the tolerances used in the analyses have been obtained considering the achievable tolerances by the

Table 3. Fabrication and Assembling Tolerance Budget

PM radius	±2 mm	Test plate fit N	1 fringes
PM conic	±0.001	Irregularity ΔN	0.2 fringes
PM RMS figure error	λ/27	Air spacing	±0.02 mm
SM radius	±0.5 mm	Lens thickness	±0.02 mm
SM conic	±0.001	Lens wedge	±0.02 mm
SM RMS figure error	λ/34	Lens tilt	±1′
SM tilt	±5″	Lens decenter	±0.02 mm
SM decenter	±0.01 mm	Refractive index	±0.001
Focal plane tilt	±10″	Abbe number	±0.8%

Dichromatic ray-splitting prism tolerances

N	ΔN	Parallel error	Thickness	Tilt
1	0.2	±1′	±0.05 mm	±1′

Table 4. Estimated Spot Size of Monte Carlo Tolerance Analysis

	Diameter of 80% or 70% EE (pixel)	
FOV	Design	Design + Tolerance
Blue band of VT	1.29–1.43 (80% EE)	1.43–1.6 (80% EE)
Red band of VT	1.56–1.60 (70% EE)	1.69–1.78 (70% EE)
FGS	1.68–2.21 (80% EE)	1.81–2.68 (80% EE)

manufacturing and assembling processes. The fabrication and assembling tolerances are shown in Table 3. A Monte Carlo analysis with 1000 run has been done to estimate the optical performance of the telescope, the results of which are shown in Table 4 [9]. The tilt and decenter of the SM are tightened to ±5 in. and ±0.01 mm in order to guarantee the required optical performance.

5. THERMAL ANALYSIS

The curvatures and shapes of the mirrors and the distance between them, the curvatures, thicknesses, and refractive indices of lenses will change with temperature. Those changes will degrade the optical performance of the VT. In order to provide the prime requirement for the thermal design, the working temperature range for the VT has been analyzed.

The opto-mechanical materials for the VT have been chosen carefully in order to reduce its sensitivity to the temperature. SiC has been used for the two mirrors. For the SM spider structure and the barrel between the PM and the SM, the carbon fiber reinforced plastic (CFRP) composites material has been used. The after-optics supports, such as the lens and prism supports, the spacers, and the focal plane assembly supports are made of titanium alloy. The thermal expansion coefficients of materials used in the VT are shown in Table 5.

The temperature is assumed to be constant for all the elements in the thermal analysis. To analyze the optical performance in the range of 15°C–25°C, the encircled energy has been used. The performances of all FOVs have been calculated on the same focal plane, without any focusing adjustment with respect to the nominal 20°C condition.

Table 5. Thermal Expansion Coefficients of Materials Used in the VT

Elements	Materials	Thermal Expansion Coefficients (10^{-6}/°C)
PM, SM	SiC	2.6
Lens 1, Windows	Fused silica	0.5
Lens 2, Lens 3	HLAK3	6.2
Prism	HZK3	6.1
Barrel, SM spider	CFRP	1
After-optics supports	Titanium	8.9

Figure 12 shows the EE curves due to temperature changes in the 20°C ± 5°C range. It can be seen that the working temperature should be kept between 17°C–23°C in order to keep the optical performance.

The temperature gradients have been taken into consideration and their effects to the optical performance have been analyzed. In order to satisfy the EE specifications, the radial and axial temperature gradients of the PM and the barrel should be kept below 2°C.

6. STRAY LIGHT DESIGN AND ANALYSIS

The SVOM satellite will be launched into a circular orbit at an altitude of around 630 km and an inclination of around 30°. A specific pointing law has been adopted in order to avoid permanent known X sources, such as galactic equator and SCOX1. Figure 13 shows the satellite pointing strategy and its relationship with the Sun and Earth [10].

The VT is mounted on the $+X$ side of the SVOM satellite. The line of sight of the telescope coincides with the $+X$ direction of the spacecraft. The Z axis of the satellite is perpendicular to the orbit plane. The Sun is kept 90°away from the $+X$ axis and no more than 90° away from the $+Z$ axis of the satellite. The angle between the Sun and the YZ plane of the satellite is kept below 5°. In normal observation mode, the VT only works on the nightside of the Earth and the Sun should always be kept behind the telescope in order to fulfill the observation and safety requirements.

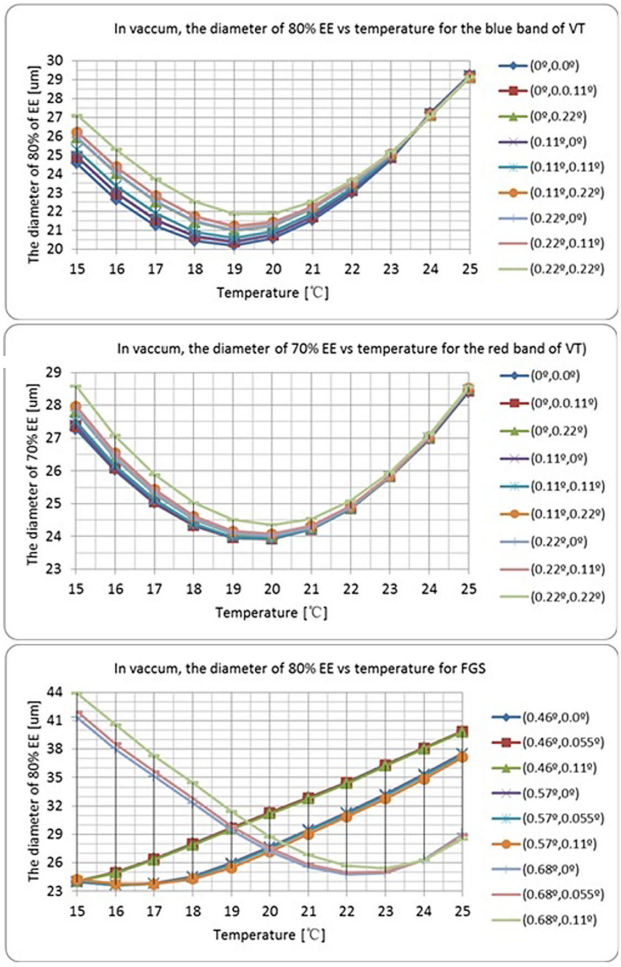

Fig. 12. Diameter of the EE versus temperature: blue band of the VT (top), red band of the VT (middle), and the FGS (bottom).

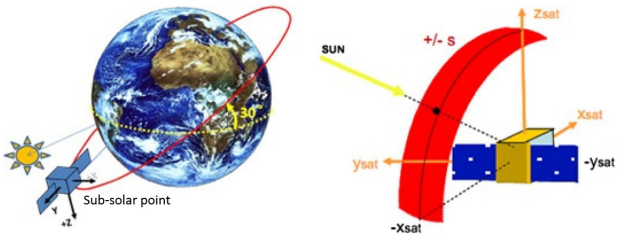

Fig. 13. Relationship between the SVOM satellite and the Sun: sub-solar view (left) and the pointing coordinate of the satellite versus the Sun (right).

A. Stray Light Requirements

Based on the anti-solar pointing observation strategy, which keeps the Sun behind the telescope, the sunlight will not directly illuminate the interior of the VT, but the sunlight scattered by the stars, Moon, and Earth will probably enter in the VT and cause serious stray light problems. The zodiacal light is an inescapable stray light background.

In order to reach the limiting magnitude of +22.5 Mv, the requirement for the mean stray light level on the detectors is such that the scattered light from the Moon should be reduced to less than 1/3 of the sky background in the imaged area of the sky when the Moon is 30 deg off the optical axis of the telescope.

The brightness of the full Moon out of the atmosphere is about −12.7 Mv and its illuminance at the entrance port of the VT is given by [11]

$$E_{\text{Moon}} = 0.3079\, lx. \tag{1}$$

The brightness of the sky background is about +22.4 Mv/arcsec^2 and its illuminance on the focal plane of the VT can be defined as

$$E_{\text{skybackground}} = E_{+22.4\,\text{Mv}} \cdot 0.77^2 \cdot \tau \cdot \left(\frac{D}{\mu}\right)^2 = 1.06 \times 10^{-6}\, lx$$
$$\left(E_{+22.4\,\text{Mv}} = 2.804 \times 10^{-15}\, lx,\ \tau = 0.6,\ D = 440\ \text{mm},\ \mu = 0.0135\ \text{mm}\right), \tag{2}$$

where 0.77 is the pixel resolution (in the unit arcsecond), τ is the optical transmission of the VT, D is the diameter of the entrance pupil, and μ is the pixel size.

The point source transmittance (PST) is adopted to evaluate the stray light level of the VT, which is defined as the illuminance on the focal plane divided by the source illuminance at the entrance port. In order to meet the stray light requirement, the PST can be written as

$$E_{\text{skybackground}}/3 > E_{\text{Moon}} \times \text{PST} \times \cos\theta, \tag{3}$$

where θ is the off-axis angle. Finally, the PST at the 30 deg off-axis angle is given by

$$\text{PST}_{30\,\text{deg}} < 1.32 \times 10^{-6}. \tag{4}$$

B. Baffles

Baffles are employed to eliminate the direct light than can reach the detector without any scattering. For a two-mirror optical system, the most common baffles are external baffle and the internal baffles near the mirrors. Optimal baffles not only eliminate the direct hostile rays, but also keep the obscuration caused by the SM assembly as small as possible. It is highly desirable that the external baffle shield the PM surface from the direct Moon or Earth illumination. The length of the baffle is determined by the angle between the stray light source and the optical axis [12].

The length of the external baffle is about 515.5 mm and the internal aperture of the first vane is Φ466 mm. The stray light source outside the 24° off-axis angle cannot illuminate the PM directly. The internal PM and SM baffles have been designed to attenuate the stray light that can reach the detector directly. The length of the PM internal baffle is 195 mm and the length of the SM baffle is 65 mm, both measured from the vertex of each mirror. The baffle vanes are also designed according to the two-reflect design law, which requires the incident light to be reflected two times before reaching the PM. The baffles and vanes designs are shown in Fig. 14 [13].

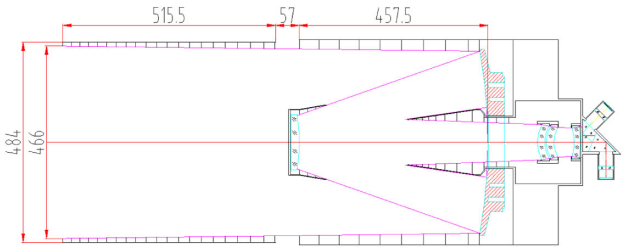

Fig. 14. Structure of the baffles and vanes.

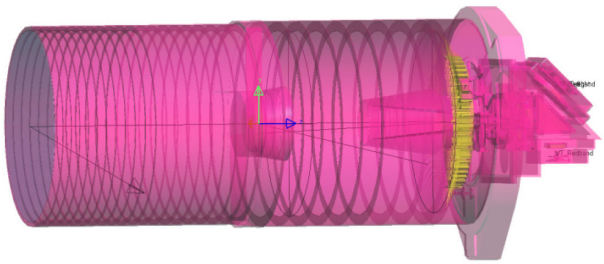

Fig. 15. Stray light analysis model of the VT.

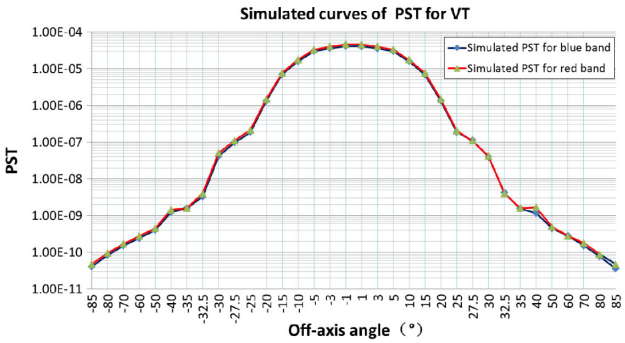

Fig. 16. Simulated PST curves for the VT.

C. Stray Light Modeling and Analysis

Stray light modeling is critical for the stray light analysis. To improve the ray-tracing accuracy, all the optical and mechanical geometries are imported from the real structure into the optical ray-trace software [14]. All the surface properties, such as optical coatings and black paint, use the measured data. The stray light model of the VT is shown in Fig. 15.

The PST is adopted here for stray light analysis. The point source is assumed to be at infinite distance and the collimated rays from −85° to 85° off-axis angles that fill the whole aperture are traced. The PST at each angle is calculated and shown in Fig. 16. The PSTs at ±30° off-axis angles are less than 5E-8 for the blue band and red band of the VT. The stray light suppression requirement has been met.

7. PERFORMANCE VALIDATION

A. RMS WFE Test

The RMS WFE of the assembled telescope is measured using a ZYGO interferometer and a flat mirror. The measured RMS WFE of the on-axis FOV is 0.055λ (λ = 632.8 nm), which is shown in Fig. 17. For the whole FOV, the maximum RMS WFE is 0.06λ. It can be seen that the VT has a good optical performance.

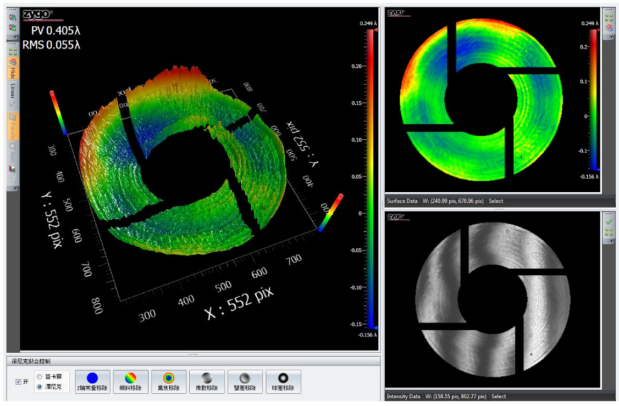

Fig. 17. Measured RMS WFE for on-axis FOV of the VT.

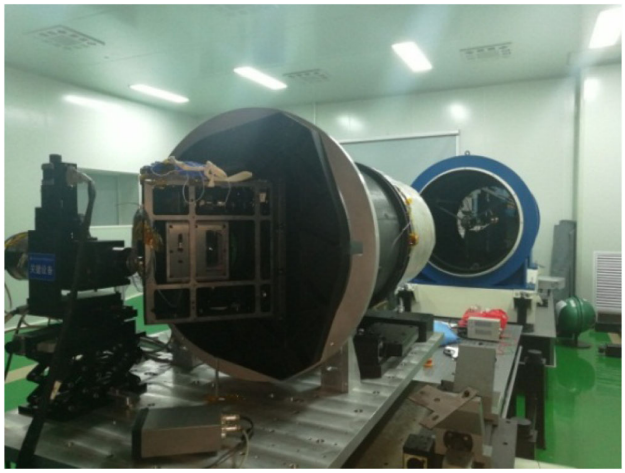

Fig. 18. VT under EE testing in the lab.

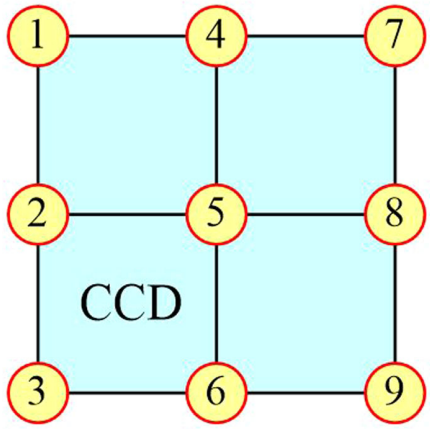

Fig. 19. Tested points of the FOV on each CCD.

Table 6. EE Test Results for the VT and FGS

FOV points	1	2	3	4	5	6	7	8	9
VT blue band (pixel)	1.73	1.35	1.35	1.35	1.16	1.54	1.36	1.35	1.73
VT red band (pixel)	1.65	1.61	1.73	1.62	1.58	1.62	1.73	1.61	1.65
FGS1 (pixel)	2.2	1.8	1.4	1.6	1.4	1.6	1.8	1.4	1.6
FGS2 (pixel)	1.8	1.8	1.8	2	1.8	1.8	2	1.8	2

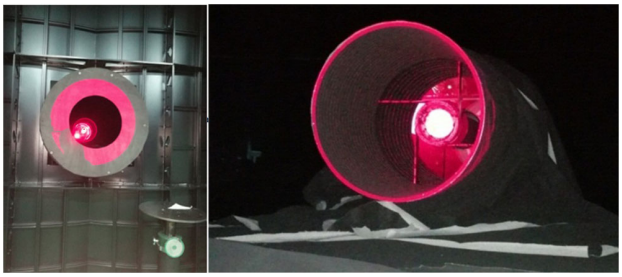

Fig. 20. Entrance port of the double cylindrical chamber (left) and VT under PST test (right) in the lab.

B. Encircled Energy Test

The telescope is finally tested using a collimator with a focal length of 20 m in the lab. A Φ0.02 mm star tester is placed on the focal plane of the collimator to simulate a point source in the infinite distance. Figure 18 shows the telescope under EE testing in the lab.

Nine FOV points for each CCD are tested (Fig. 19). The test results are shown in Table 6. The diameters of 80% (blue band) or 70% (red band) of EE for the VT are no more than 1.73 pixels. For the FGS, the diameters of 80% EE are all smaller than 2.2 pixels.

C. PST Test

The PST of the VT is tested after the opt-mechanical assembling process in the stray light test facility. A collimator with a laser source is employed to simulate the infinite point source. The telescope is put on a rotating table in the double cylindrical chamber [15,16]. A stop is located outside the entrance port to prevent the useless light entering the chamber. The VT under PST testing in the lab is shown in Fig. 20.

Figure 21 shows the tested and simulated PST curves for the dual band of the VT. It can be seen that the tested and simulated PST curves are in good agreement between ±10° and ±30° off-axis angles. The PSTs at ±30° off-axis angle are all less than 2E-7 for the dual band of the VT, so the stray light suppression requirement has been met.

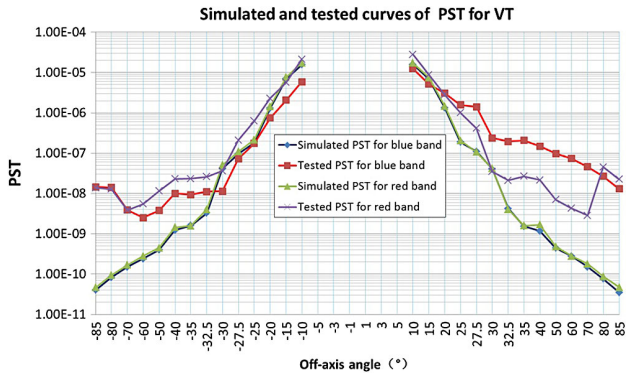

Fig. 21. Simulated and tested PST curves for dual band of the VT.

The departure in the tested and simulated PST occurs at the small off-axis angles below 10° and the large off-axis angels above 35° due to the noise errors of the PST test system that will be minimized in the future.

8. CONCLUSIONS

The optical design of the VT for the SVOM mission is presented in this paper. The VT can provide 0.77 arc sec pixel resolution images of the afterglows of GRBs from the visible to the near-infrared at the same time. The design concept is based on a 0.44 m modified Ritchey–Chrétien telescope with a dichroic ray-splitting prism. The optical system is as compact as possible near the primary mirror to provide good stability. Two FGS CCDs are arranged on the visible focal plane beside the main CCD sensor to improve the pointing precision of the satellite. SiC mirrors are adopted with a great lightweight design that is critical to reduce the mass of the telescope. A focalizing method using the first two lenses is designed to ensure the telescope's optical performance in orbit. A reasonable tolerance error budget is given to make sure the telescope can be correctly built. Thermal analysis shows the optical performance can be maintained when the temperature of the VT is kept in the range of 20°C ± 3°C. The optical performance is validated in the lab and the PST simulation and testing show that the baffles and vanes are effective, and the stray light design meets the scientific requirement.

At the time of writing, the telescope has completed all the performance testing both in the lab and outdoor observations. The telescope now is undergoing the integration and testing with the satellite, which is scheduled to be launched in 2021.

Disclosures. The authors declare no conflicts of interest.

REFERENCES

1. O. Godet, J. Paul, J. Y. Wei, S.-N. Zhang, J.-L. Atteia, S. Basa, D. Barret, A. Claret, B. Cordier, J.-G. Cuby, Z. Dai, F. Daigne, J. Deng, Y. Dong, D. Götz, J. Hu, P. Mandrou, J. P. Osborne, Y. Qiu, J. Wang, B. Wu, C. Wu, and W. Yuan, "The Chinese-French SVOM Mission: studying the brightest astronomical explosions," Proc. SPIE **8443**, 844310 (2012).
2. F. Gonzalez and S. Yu, "SVOM: a French/Chinese cooperation for a GRB mission," Proc. SPIE **10699**, 1069920 (2018).
3. C. Amoros, B. Houret, K. Lacombe, V. Waegebaert, J.-L. Atteia, A. Bajat, L. Bautista, I. Belkacem, S. Bordon, B. Cordier, M. Galliano, O. Godet, F. Gonzalez, Ph. Guillemot, S. Maestre, P. Mandrou, W. Marty,

R. Pons, D. Rambaud, and P. Ramon, "Status of technological development on ECLAIRs camera onboard the SVOM space mission," Proc. SPIE **10699**, 106995K (2018).
4. K. Mercier, F. Gonzalez, D. Götz, M. Boutelier, N. Boufracha, V. Burwitz, M. C. Charmeau, P. Drumm, C. Feldman, A. Gomes, J. M. Le Duigou, N. Meidinger, A. Meuris, P. O'Brien, J. Osborne, P. Pasqier, L. Perraud, J. F. Pearson, F. Pinsard, E. Raynal, and R. Willingale, "MXT instrument on-board the French-Chinese SVOM mission," Proc. SPIE **10699**, 1069921 (2018).
5. H. Gross, F. Blechinger, and B. Achtner, *Handbook of Optical System*, Volume **4**: Survey of Optical Instruments (Wiley, 2008), Chap. 43.
6. L. Feinberg, L. Cohen, B. Dean, W. Hayden, J. Howard, and R. Keski-Kuha, "Space telescope design considerations," Opt. Eng. **51**, 011006 (2012).
7. J. W. Figoski, "Design and tolerance specification of a wide-field three-mirror, unobscured, high-resolution sensor," Proc. SPIE **1049**, 157–165 (1989).
8. M. Zusi, R. Paolinetti, V. Della Corte, G. Marra, M. Baroni, P. Palumbo, and G. Cremonese, "Optical design of the high resolution imaging channel of SIMBIO-SYS," Appl. Opt. **58**, 4059–4069 (2019).
9. Y. Qin and H. Hua, "Optical design and system engineering of a multiresolution foveated laparoscope," Appl. Opt. **55**, 3058–3068 (2016).
10. Y. She and S. Li, "Optimal slew path planning for the Sino-French Space-based multiband astronomical Variable Objects Monitor mission," J. Astron. Telescope Instrum. Syst. **4**, 017001 (2018).
11. D. C. Agrawal, "Apparent magnitude of earthshine: a simple calculation," Eur. J. Phys. **37**, 035601 (2016).
12. V. Y. Terebizh, "Optimal baffle design in a Cassegrain Telescope," Exp. Astron. **11**, 171–191 (2001).
13. M. S. Kumar, C. S. Narayanamurthy, and A. S. K. Kumar, "Iterative method of baffle design for modified Ritchey-Chretien Telescope," Appl. Opt. **52**, 1240–1247 (2013).
14. V. Isbrucker, J. Stauder, D. Laurin, and A. Hollinger, "Stray light control for asteroid detection at low solar elongation for the NEOSSat micro-satellite telescope," Proc. SPIE **8442**, 84424J (2012).
15. J. Fleming, F. Grochocki, T. Finch, S. Willis, and P. Kaptchen, "New stray light test facility and initial results," Proc. SPIE **7069**, 70690O (2008).
16. F. Grochocki and J. Fleming, "Stray light testing of the OLI Telescope," Proc. SPIE **7794**, 77940W (2010).